Title: Beta cell hubs dictate pancreatic islet responses to glucose

Authors: Natalie R. Johnston[1], Ryan K. Mitchell[1], Elizabeth Haythorne[1], Maria Paiva Pessoa[1], Francesca Semplici[1], Jorge Ferrer[2], Lorenzo Piemonti[3], Piero Marchetti[4], Marco Bugliani[4], Domenico Bosco[5], Ekaterine Berishvili[5], Philip Duncanson[6], Michael Watkinson[6], Johannes Broichhagen[7], Dirk Trauner[7], Guy A. Rutter[1]* and David J. Hodson[1,8,9]*

Affiliations: [1]Section of Cell Biology and Functional Genomics, Division of Diabetes, Endocrinology and Metabolism, Department of Medicine, Imperial College London, London W12 0NN, UK. [2]Beta Cell Genome Regulation Lab, Department of Medicine, Imperial College London, London W12 0NN, UK. [3]Diabetes Research Institute (HSR-DRI), San Raffaele Scientific Institute, Via Olgettina 60, 20132 Milan, Italy. [4]Department of Clinical and Experimental Medicine, Islet Cell Laboratory, University of Pisa, Pisa, Italy. [5]Cell Isolation and Transplantation Center, Department of Surgery, Geneva University Hospitals and University of Geneva, Geneva, Switzerland. [6]School of Biological and Chemical Sciences, Queen Mary University of London, Mile End Road, London, E1 4NS, UK. [7]Department of Chemistry, Ludwig-Maximilians-Universität München, and Munich Center for Integrated Protein Science, Butenandtstrasse 5-13, 81377 München, Germany. [8]Institute of Metabolism and Systems Research (IMSR), University of Birmingham, Edgbaston, B15 2TT, UK. [9]Centre for Endocrinology, Diabetes and Metabolism, Birmingham Health Partners, Birmingham, B15 2TH, UK.

*Correspondence to:
d.hodson@imperial.ac.uk
d.hodson@bham.ac.uk
g.rutter@imperial.ac.uk

Word count (excluding eTOC, highlights, summary, acknowledgements and contributions):
57,796

Key words: islets, insulin, beta cells, diabetes, optogenetics, imaging

HIGHLIGHTS

- Optogenetic and photopharmacological targeting reveals a pacemaker-like beta cell subpopulation
- These cells, termed hubs, are required for normal insulin release
- Photopainting demonstrates that hubs are highly metabolic and transcriptionally immature
- Hubs are targeted by a diabetic milieu to induce islet failure

eTOC Blurb

Using advanced imaging approaches, Johnston et al show that a few (1-10%) beta cells exert disproportionate control over islet responses to glucose. These specialized cells, termed hubs, are partly immature and highly metabolic. Their failure during type 2 diabetes mellitus may lead to reduced insulin secretion and impaired glucose homeostasis.

SUMMARY

The arrangement of beta cells within islets of Langerhans is critical for insulin release through the generation of rhythmic activity. A privileged role for individual beta cells in orchestrating these responses has long-been suspected, but not directly demonstrated. We show here that the beta cell population *in situ* is operationally heterogeneous. Mapping of islet functional architecture revealed the presence of hub cells with pacemaker properties, which remain stable over recording periods of 2-3 hours. Using a dual optogenetic/photopharmacological strategy, silencing of hubs abolished coordinated islet responses to glucose, whereas specific stimulation restored communication patterns. Hubs were metabolically-adapted and targeted by both pro-inflammatory and glucolipotoxic insults to induce widespread beta cell dysfunction. Thus, the islet is wired by hubs, whose failure may contribute to type 2 diabetes mellitus.

INTRODUCTION

The release of insulin from pancreatic beta cells is necessary for proper glucose homeostasis in mammals. Beta cells respond to glucose with increased oxidative metabolism, elevations in cytosolic ATP/ADP ratio and closure of ATP-sensitive K^+ (K_{ATP}) channels (Rutter et al., 2015). The consequent plasma membrane depolarization activates voltage-dependent Ca^{2+} channels (VDCC), leading to Ca^{2+} influx and exocytosis of secretory granules (Rutter et al., 2015).

The three-dimensional organization of beta cells is also important for the normal regulation of insulin secretion. Thus, beta cells throughout the islet microorgan display rhythmic activity patterns in the presence of high glucose (Benninger et al., 2008; Santos et al., 1991). A role for specialized beta cells in orchestrating these dynamics has long been postulated, including the presence of putative 'pacemakers' (Ämmälä et al., 1991; Benninger et al., 2014; Squires et al., 2002). Indeed, isolated beta cells possess discrete metabolic characteristics and secretory profiles (Katsuta et al., 2012; Kiekens et al., 1992; Salomon and Meda, 1986), and phase lags in the onset of electrical activity can be detected between distant islet regions (Benninger et al., 2008; Meda et al., 1984; Palti et al., 1996). More recent studies have revealed functional differences between hundreds of individual beta cells monitored *in situ* in the intact islet (Hodson et al., 2013; Li et al., 2011; Stozer et al., 2013). Such heterogeneity may be relevant for type 2 diabetes pathogenesis, since specific insults might target single cells or defined islet regions to induce insulin secretory failure. However, whether particular subsets of cells drive the behavior of others has so far been difficult to prove empirically.

Over the past decade, optogenetics has allowed reversible control of neuronal activity with light (Zhang et al., 2007). In parallel, photopharmacology has harnessed the power of azobenzene photoresponsive units to produce exogenously-applied compounds that turn ion channels and G-protein-coupled receptors into endogenous photoswitches (Broichhagen et al., 2015). As both these approaches are applicable to electrically-excitable endocrine tissue (Broichhagen et al., 2014; Reinbothe et al., 2014), they afford the unique opportunity to precisely manipulate cell activity with high spatiotemporal fidelity. Using all-optical interrogation of individual beta cells *in situ*, we therefore set out to probe the topology that regulates population glucose responsiveness, with the aim of identifying the islet-resident pacemaker.

RESULTS

Hubs are a feature of beta cell population dynamics

To visualize the large-scale organization of beta cell activity underlying calcium (Ca^{2+})-dependent exocytosis of insulin granules, intact mouse islets were subjected to high-speed (2-8 Hz) multicellular Ca^{2+}-imaging (Hodson et al., 2012). This was combined with Monte Carlo-based correlation analyses in which repeated shuffling of Ca^{2+}-events (> 9999 iterations) is used to determine whether cells are coordinated due to chance or not (*i.e.* contributing to the same insulin release event). Together, these approaches allow online mapping of the islet functional circuitry. Initial experiments confirmed that beta cells form a scale-free network (Stozer et al., 2013) that supports the synchronous propagation of glucose (11 mM)-stimulated Ca^{2+} waves by efficiently connecting distant islet regions (R^2 = 0.72; Fig. 1A). Scale-free networks are ubiquitous throughout biology, are identified by their power-law link-probability distribution (Hodson et al., 2010), and adopt a hub and spoke formation where a few cells possess the majority of connections. Accordingly, a stereotypical feature of such topology in islets was the non-random appearance of rare super-connected hubs, whose firing activity tended to repetitively precede and outlast that of the remainder of the population (*i.e.* was pacemaker-like) (Fig. 1B and C) (Movie S1).

Such islet architecture was dependent on information exchanges through gap junctions, since reversible blockade of connexin channels using 18α-glycyrrhetinic acid (AGA) (Farnsworth et al., 2014) reduced the number of hubs, decreased coordinated population activity, and increased signal propagation path length (Fig. 1D-G). This may reflect the inability to identify hubs due to loss of cell-cell entrainment, as well as re-routing of information over longer distances by the remaining hubs. Notably, no differences in the amplitude of Ca^{2+} rises were seen in control and AGA-treated tissue (Fig. S1A-C), suggesting minimal impact upon VDCC activity. In all cases, parallel experiments were performed using glycyrrhizic acid (BGA), the inactive precursor of AGA that exerts similar non-specific effects (Desarmenien et al., 2013). Results could be replicated using mebeverine (Farnsworth et al., 2014) (Fig. S1D), a gap junction inhibitor with no reported effects on VDCC or K_{ATP} channel activity, as well as *Gjd2* shRNA to specifically silence connexin 36 at the islet surface (Fig. S1E-H).

Hubs are stable and present across species

To assess network topology stability, islets were recorded and then left on the microscope for between 30 mins and 3 hrs before re-recording. Network topology was stable both over time and in response to perturbation, as statistically assessed *versus* a third experiment subjected to either randomization (*i.e.* to re-distribute the wiring pattern) or enforced-dissimilarity (*i.e.* to form a different wiring pattern) (Fig. 1H and I). Network indices were unaffected in the presence of either a specific glucagon receptor antagonist (Fig. S1I and J) or a glucagon-neutralizing antibody (Fig. S1K and L), suggesting that any glucagon present *in vitro* is unlikely to influence hub function. Hinting at a conserved role for hub architecture, islet functional topologies were similar in glucose-stimulated mouse and human islets, as shown by the similar link-probability distributions (*i.e.* both are fitted with a power-law of near-identical exponent value). However, synchrony tended to be compartmentalized into subregions/clusters in human islets (Fig. 1J), in line with the different structural arrangement of beta- *versus* alpha-cells in this species (Bosco et al., 2010). Beta cell Ca^{2+} responses were not dependent on orientation toward the islet center or periphery (ΔY Fluo2 = 0.14 ± 0.01 *versus* 0.13 ± 0.004 AU, periphery *versus* center, respectively), and identical results were obtained using the genetically-encoded indicator GCaMP6 (Fig. 1K and L), engineered to interfere less with intracellular Ca^{2+} levels.

A strategy for all-optical interrogation of beta cell function

To functionally dissect the role of hubs, an optogenetic strategy was developed and validated, enabling electrical silencing following *Ins1Cre*-directed expression of the light-gated chloride (Cl^-) pump halorhodopsin (eNpHR3.0) (Zhang et al., 2007) in beta cells (Fig. 2A and B). This

approach allowed the reversible silencing of single beta cell or population Ca^{2+}-spiking activity and extracellular Ca^{2+} influx following illumination (λ = 560-590 nm) (Fig. 2C-G) (Movies S2-4). Application of the depolarizing agent potassium chloride was able to overcome silencing by restoring VDCC activity (Fig. 2H). Of note, wild-type beta cells were refractory to silencing (Fig. 2I and J), and eNPHR3.0-expressing beta cells under irradiation were not further hyperpolarized using diazoxide to force open K_{ATP} channels (Fig. 2K). As measured using patch-clamp electrophysiology, illumination induced photocurrents (Fig. 3A), leading to membrane hyperpolarization and electrical silencing only in eNPHR3.0-expressing beta cells (Fig. 3B-D). Thus, specific and powerful optogenetic silencing could be achieved.

Animals harboring a single eNpHR3.0 allele unexpectedly demonstrated improved glucose tolerance compared to wild-type littermates, despite normal insulin sensitivity (Fig. 4A-F) and body weight (Fig. 4G and H). This was probably due to enhanced *in vivo* insulin secretion (Fig. 4I), as beta cell mass was apparently normal (Fig. 4J). Activation of eNpHR3.0 on an Ins1Cre background also led to similar results, suggesting that alternation in insulin gene dosage in the context of the transgene was unlikely to be a contributing mechanism (Fig. 4K and L). Pertinent to the *in vitro* studies here, however, isolated islets responded normally to glucose in terms of ionic fluxes and insulin release (Fig. S2A-I), and eNpHR3.0 does not possess basal activity in the absence of light (Zhang et al., 2007) (also shown in Fig. 3C).

Hubs orchestrate beta cell population responses to glucose

By performing analysis in real-time using islets maintained on the microscope stage, hubs could be identified and subsequently manipulated (Fig. 5A-C). Silencing of individual hubs using a pinpointing laser had catastrophic consequences for coordinated islet responses to high glucose (Fig. 5D and E) (Movies S5-6), an effect reversed simply by ceasing illumination (Fig. 5F and G). The strength of inhibition following targeting of individual hubs tended to be inversely associated with the number of these cells per islet before silencing (Fig. S2J), suggesting that some redundancy is present in the system, most likely due to follower cells being controlled by more than one hub. By contrast, silencing of individual non-hub or follower cells did not significantly perturb islet dynamics (Fig. 5H), demonstrating the specificity of the approach.

Using a similar technique, hubs were firstly identified at high glucose, before inactivation using low glucose and stimulation with JB253, an exogenously-applied K_{ATP} channel photoswitch based on glimepiride (Broichhagen et al., 2014). Following targeted illumination of JB253-treated islets, hub connectivity could be mimicked without activation of intervening cells, as determined by the presence of glucose- and gap junction-dependent entrainment patterns in follower cells (conduction velocity = 47.0 ± 8.9 μm/s) (Fig. 5I-K). Such effects were unlikely to stem from diffusion of active JB253, since this molecule turns off within milliseconds in the dark (Broichhagen et al., 2014), and proximate cells remained unaffected by hub stimulation (Fig. S3).

Hubs are required for insulin secretion

We were unable to measure insulin secretion accurately from a single islet over the 5 min experimental period used here, since levels were below the detection sensitivity of current assays. Therefore, to link hub activity with hormone release, the cell-surface-attached fluorescent Zn^{2+} probe JP-107 (Pancholi et al., 2014) was instead employed as a surrogate to dynamically report Zn^{2+} co-released with insulin from cells at the islet surface, as previously reported with ZIMIR (Li et al., 2011). Using this approach, silencing of follower cells or wild-type islets was without effect, as evidenced by a linear increase in fluorescence due to Zn^{2+} accumulation at the probe. By contrast, hub shutdown or global illumination lowered insulin/Zn^{2+} release to below the dissolution rate of the probe (*i.e.* Zn^{2+} binding is lower than Zn^{2+} removal) (Fig. 5L).

While it was not technically possible to directly link hub activity with pulsatile insulin release, the acetocholinomimetic carbachol (Zhang et al., 2008a) was able to accelerate beta cell population activity (Fig. S3E), without altering the proportion of links or hubs (Fig. S3F, G). Moreover, rapid imaging performed over dozens of minutes- *i.e.* within the range of insulin

pulses (Head et al., 2012)- revealed that hubs are also a feature of population behavior over longer periods (proportion hubs = 7.1 ± 1.3%; proportion links = 9.7 ± 2.0%). Since carbachol has been shown to phase-set activity between islets *in vitro* (Zhang et al., 2008a), parasympathetic neurons may plausibly target hubs *in vivo* to synchronize islet activity and generate insulin pulses.

Hubs possess a characteristic metabolic signature

We next sought to understand what makes a hub cell unique. Islet-wide Ca^{2+} signals were recorded before metabolic profiling of the hub population in the same islet using the mitochondrial potential dye tetramethylrhodamine ethyl ester (TMRE), which sequesters in active, hypeporlarized mitochondria. Following stimulation at high glucose, mitochondria in hubs became more hyperpolarized *versus* those in non-hubs (Fig. 6A and B), suggesting increased proton-pumping, ATP synthase activity and ATP generation (Tarasov et al., 2012). While the duty cycle (*i.e.* proportion of time the cell spends 'ON') was slightly increased in hubs compared to non-hubs (Fig. 6C), other activity parameters including Ca^{2+}-spiking amplitude and frequency were broadly similar (Fig. 6D-F). Spatially, hubs and non-hubs were intermingled, with no clear preference for the islet center or periphery detected for either population based on polar coordinates (angle and distance taken from the islet center) (Fig. 6G and H).

Hubs display features of both mature and immature beta cells

Using photoactivatable Tag-RFP (PA-TagRFP) to photopaint single hubs within islets using a 405 nm laser (Fig. S4A and B), post-hoc immunostaining against a variety of markers of beta cell 'identity' (Rutter et al., 2015) could be performed (Fig. 6I), without adversely altering Ca^{2+} dynamics (Fig. S4C). These studies revealed reduced insulin content, increased glucokinase (GK/*Gck*) levels, lowered expression of pancreatic duodenum homeobox-1 (*Pdx1*), but normal levels of the mitochondrial import receptor subunit Tom20 in hubs *versus* the rest of the population (Fig. 6I and J) (Fig. S5). The transcription factor Nkx6.1, recently shown to be required for insulin biosynthesis and beta cell proliferation (Taylor et al., 2013), was almost absent from hubs (Fig. 6I and J). Suggesting that hubs are unlikely to represent a multihormonal (*e.g.* Glu+, Ins+) population, no co-localization with glucagon was detected (Fig. 6K). Likewise, neurogenin-3, a beta cell precursor marker , was undetectable at the protein level in the adult islet, implying that hubs are unlikely to be trapped in a progenitor state (Fig. 6K). Inspection of oversampled and deconvolved superresolution confocal images revealed no differences in mitochondrial distribution/shape or endoplasmic reticulum content in hubs (Fig. 6L-P), although expression of the sarco(endo)plasmic reticulum Ca^{2+}/ATPase, SERCA2, was markedly reduced (Fig. 6O and P).

Suggesting a hyposecretory (or degranulated) nature, insulin granule numbers were lower in hubs *versus* non-hubs, despite a similar distribution (Fig. 6Q and R). Furthermore, the area of individual hub cells was comparable to the rest of the population (range = 122-381 μm^2 and 194-355 μm^2, non-hubs *versus* hubs, respectively), and their shape appeared to be normal. Consequently, hubs constitute a metabolically-adapted, repurposed subpopulation of beta cell which displays features of immature cells.

Hubs are targeted by diabetic milieu

Lastly, the robustness of hubs was determined by challenging islets with cytokine cocktails (IL-1β/IL-6, or IL-1β/TNF-α) to re-create the pro-inflammatory milieu thought to be associated with diabetes (O'Neill et al., 2013). Acutely, the application of cytokines led to a large ramp-up in Ca^{2+} spiking activity in the presence of high glucose (Fig. S6). However, after only 2 h incubation, a collapse in hub cell number was apparent (Fig. 7A and B), and this could be viewed in real-time by recording the same islet left *in situ* before and during exposure to cytokine (IL-1β/IL-6) (Fig. 7C and D). The cytokine-induced disruption to hub cell function was further evidenced by a reduction in the number of cells occupying the upper or 'high connectivity' region of the link-

probability distribution (Fig. 7E and F), as shown by a decrease in the exponent value of the power-law fit. This resulted in a dramatic decline in correlated beta cell population function (Fig. 7G) due to the presence of fewer and less well-connected hubs. The actions of cytokines were not explained by effects on cell viability, as assessed using indices of necrosis (Fig. 7H and I) and apoptosis (Fig. 7J). However, 2 h cytokine exposure decreased mRNA levels of the major islet gap junction isoform connexin 36 (*GJD2*) three-fold (Fig. 7K and L), and this was already associated with a substantial reduction in gap junction plaque number (Fig. 7M), in line with that recently reported using a similar paradigm (Farnsworth et al., 2015). Likewise, preferential hub failure was detected in both rodent and human tissue in response to gluco(lipo)toxic insults (Fig. 7N and O).

DISCUSSION

Beta cells are a phenotypically diverse population, presenting a mosaic of metabolic and electrical activity patterns (Pralong et al., 1990), which is mirrored at the level of insulin secretory capacity (Katsuta et al., 2012; Kiekens et al., 1992; Li et al., 2011; Salomon and Meda, 1986). When viewed as a population, beta cells are often termed a functional syncytium, although a role for cell heterogeneity in generating multicellular dynamics has been invoked repeatedly (Benninger and Piston, 2014; Stozer et al., 2013). Indeed, it has been shown that a subset (~10-15 %) of beta cells may exert a disproportionate influence over islet dynamics (Hraha et al., 2014). By combining large-scale functional cell mapping with optogenetics and photopharmacology, we provide here a revised blueprint for islet function whereby a few pioneer hubs with reduced beta cell identity dictate emergent population behavior in response to glucose. Importantly, hub topologies are a feature of dynamical systems, including cell networks in the brain and pituitary (Bonifazi et al., 2009; Hodson et al., 2012), since they are functionally robust at a low wiring cost (Bullmore and Sporns, 2009) (*i.e.* the chances of randomly hitting a hub are low). However, should a hub be specifically targeted, the effects on cell population function are far-reaching, as observed in the islet during exposure to cytokine or glucolipotoxicity.

The present study used a single photon-based confocal system to control the activity of individual hubs or followers within isolated islets. While two photon approaches in theory increase the accuracy of cell targeting by restricting the beam to within a few microns of the focal point, there are drawbacks when used with optogenetics. Firstly, a diffraction-limited two-photon spot (*i.e.* ~ 500 nm) is insufficient to reliably activate optogenes, and the long excited state halftime can quickly saturate the rhodopsin (Rickgauer and Tank, 2009). Secondly, commercial lasers are unable to deliver the > 1100 nm excitation required for eNpHR3.0 activation without an optical-parametric oscillator (Andresen et al., 2009). By contrast, a single-photon diffraction-limited laser spot (~ 500 nm) of known absorbance cross-spectrum can be introduced to the surface of the sample, with minimal aberration and steep power drop-off as a function of $1/\text{distance}^2$. Demonstrating the high degree of localization of the effective beam, we were clearly able to photopaint single cells within an islet, and did not see any population silencing when a follower cell was targeted.

Using patch clamp recordings of dissociated beta cells, eNpHR3.0 activation hyperpolarized membrane potential by -60 mV, in line with previous reports (Mattis et al., 2012). While photocurrent size may be underestimated due to the presence of an electrochemical gradient, it should be noted that halorhodopsin derives energy from photons rather than the ion gradient itself (Pfisterer et al., 2009), and the photocycle is unaffected even in the presence of high Cl^-concentration (Varo et al., 1995). In any case, it is unlikely that hyperpolarizing spread throughout the islet *per se* could account for these observations, since: 1) only 30% of voltage spreads to an immediately coupled cell and an 86 mV depolarizing step is required for activation *via* gap junctions (Zhang et al., 2008b); and 2) stimulation of follower cells was without effect. We prefer an explanation whereby large changes in conductance attributable to the hub cell or its very close neighbors are removed through eNpHR3.0-mediated silencing, leading to impaired propagation of Ca^{2+} waves (Benninger and Piston, 2014; Benninger et al., 2008; Zhang et al., 2008b). Although membrane potential was slightly more depolarized following cessation of illumination, this is also seen in neurons (Mattis et al., 2012) and may reflect the reversal potential of Cl^-. We did not notice significant effects on hub indices during the Ca^{2+} imaging studies here due to use of a 5-10 min 'rest' period to allow Cl^- re-equilibration.

Experiments in which hub cells were stimulated revealed that hubs and followers are unlikely to form local syncytia. While the exact mechanisms for antipodal signal propagation are difficult to determine precisely, a role for 3D chains of electrically-coupled cells is plausible, given that entrainment was markedly blunted by both gap junction blockade and perfusion with 1 mM glucose. Other communication possibilities include autonomic neurons, which possess > 100 µm axonal arborizations in pancreatic slices (Rodriguez-Diaz et al., 2012), and cilia, which provide a restricted signaling corridor due to their presence in only ~ 25 % of beta cells (Gerdes

et al., 2014). Along these lines, the effect of hub silencing on islet function was surprisingly strong, given the relatively mild phenotype of animals deleted for the gap junction protein Cx36 (Ravier et al., 2005). However, considerable redundancy exists in the latter model with Cx30.2 and ephrins providing alternative signaling routes (Farnsworth and Benninger, 2014; Konstantinova et al., 2007).

An intriguing possibility is that hubs are related to the previously described Pdx1+, Ins(low) beta cell subpopulation (Szabat et al., 2009), albeit distinct in their low levels of both markers. Impaired identity, while conceivably restraining stimulus-induced secretion, may also limit GK-induced proliferation (Porat et al., 2011; Stolovich-Rain et al., 2015) to maintain the role of these cells as specialized pacemakers. Indeed, high levels of GK expression may sensitize hubs cells to increases in glucose concentration, allowing these cells to respond earlier and more robustly than their neighbours. By contrast, the failure of hubs when faced with a gluco(lipo)toxic/pro-inflammatory milieu indicates that these cells are metabolically fragile. This vulnerability might reflect high *Gck* (Roma et al., 2015) expression coupled to low Pdx1 and SERCA2 levels (Fonseca et al., 2011; Fujimoto et al., 2009), which ultimately lead to ER stress and cell dysfunction.

We acknowledge that the hub protein characterization performed here constitutes a biased screen, but it nonetheless provides a strong foundation for understanding the biology of these unusual cells. In the future, unbiased multiplex approaches, including massive parallel sequencing (RNASeq) and CyTOF (single cell mass cytometry) (Proserpio and Lonnberg, 2015), will help define the hub signature. Although attempts were made to obtain dissociated cells/cytoplasm for these purposes, PA-TagRFP fluorescence disappeared following dissociation of islets, possibly reflecting either the fragility of these cells, or the fluorophore itself. Similar problems were encountered with electron microscopy, where available antibodies cannot differentiate between activated and non-activated PA-TagRFP.

The recording approaches used to monitor hubs were technically-constrained to 2-3 h. Indeed, such experiments necessitate leaving the islets *in situ* on the microscope and re-loading with Ca^{2+} indicator, since the same field of view must be maintained for analysis purposes. Thus, it cannot be excluded that hubs may represent a transitory subpopulation that drifts over dozens of hours in line with transcriptional/translational processes. Indeed, modelling studies predict that 'pacemakers' arise from the most excitable beta cell, which is assumed to shift due to a random distribution of excitability as K_{ATP} channel expression levels vary (Benninger et al., 2014). However, the possibility that such cells may arise during development could not be excluded (Benninger et al., 2014), and studies in FACS-purified GFP-labelled beta cells suggest the presence of distinct transcriptional pools, with the proportions remaining similar between animals and days (Katsuta, Aguayo-Mazzucato et al. 2012). Moreover, to the best of our knowledge, there is no evidence that K_{ATP} channel levels change over time, though the presence of a substantial proportion of channel subunits on internal membranes (Varadi et al., 2006) may complicate such measures.

Lastly, it should be noted that experiments in isolated islets may not necessarily reflect the situation *in vivo*, where blood flow direction (beta cell -> alpha cell) (Nyman et al., 2008) and molecule access dynamics (Michau et al., 2015) may all affect the role of hubs in dictating population dynamics and insulin secretion. This possibility might be tested in the future using *in vivo* imaging approaches (Nyman et al., 2008; Speier et al., 2008).

In summary, the present findings provide new insights into the regulation of islet function by individual beta cells, and the mechanisms that likely target and impair this during type 2 diabetes pathogenesis and treatment. More generally, the paradigm developed here to study the roles of individual cells within the functioning islet may be broadly applicable to other tissues or organisms.

MATERIALS AND METHODS

Animals, glucose/insulin tolerance testing and insulin measures

Beta cell-specific expression of halorhodopsin, a light-activated hyperpolarising Cl^- pump (Zhang et al., 2007), was achieved by crossing the *Ins1Cre* deletor strain (Thorens et al., 2014) with animals engineered to express eNpHR3.0-EYFP following excision of a *loxP*-flanked STOP cassette (B6;129S-Gt(ROSA)26Sortm39(CAG-hop/EYFP)Hze/J). For detailed information see Supplemental Experimental Procedures.

Islet isolation

Animals were euthanized in a rising concentration of CO_2 before laparotomy and injection of collagenase solution (1mg/ml) into the bile duct (clamped at the duodenal ampulla). Following incubation for 10 min at 37 ^{0}C, digested pancreata were subjected to density gradient purification. Islets retrieved from the interface between the 1.083 g/ml and 1.077 g/ml layers were cultured for 24-72 h in Roswell Park Memorial Institute (RPMI) medium supplemented with 10% foetal calf serum, 100 U/mL penicillin and 100 µg/mL streptomycin.

Human islet culture

Material from heart-beating donors was obtained from isolation centres in Italy (Pisa and Milan) and Switzerland (Geneva), with necessary local and national ethical permissions, including consent from the next of kin. Islets were cultured in RPMI supplemented with 10% foetal calf serum, 100 U/mL penicillin, 100 µg/mL streptomycin, 0.25 mg/mL fungizone, and supplemented with 5.5 mM *D*-glucose. All studies involving human tissue were approved by the National Research Ethics Committee London (Fulham), REC #07/H0711/114.

Calcium and mitochondrial potential imaging

Multicellular Ca^{2+} and mitochondrial potential imaging was performed as detailed (Hodson et al., 2013). Single cell silencing in eNpHR3.0-expressing tissue was achieved using a λ = 585 nm laser (300 mW) linked *via* a single-mode fibre optic to a custom-manufactured dichroic array, configured to deliver a diffraction-limited (~ 500 nm) spot (6.8-23.4 mW/mm^2) to the focal plane (Cairn Research). Single cell stimulation was performed using the photoswitchable sulfonylurea JB253 and a diffraction-limited λ = 470 nm laser. Mitochondrial potential was monitored using TMRE. For detailed information see Supplemental Experimental Procedures.

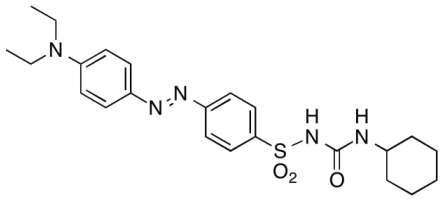

trans-**JB253**

Electrophysiology

Pancreatic islets were dissociated into single β-cells and plated onto glass coverslips. Electrophysiological recordings were performed in either perforated patch-clamp or whole-cell configuration using an EPC9 patch-clamp amplifier controlled by Pulse acquisition software (HEKA). For detailed information see Supplemental Experimental Procedures.

Dynamic insulin secretion measures

Zinc (Zn^{2+}) co-released from insulin-containing granules was measured as a proxy for insulin secretion using the chemical probe JP-107 (300 µM), as described (Pancholi et al., 2014). For detailed information see Supplemental Experimental Procedures.

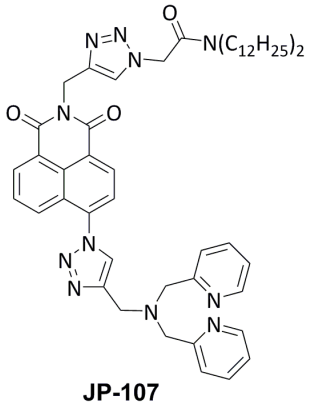

JP-107

Generation of adenoviral PA-TagRFP and photopainting

cDNA encoding the photoactivatable fluorescent protein PA-TagRFP (Subach et al., 2010) was cloned into pShuttleCMV *via Xho 1* and *Xba I* sites before recombination with pAdEasy1 and virus production as described (Luo et al., 2007). Islets were incubated for 48 h with adenovirus harboring PA-TagRFP at a multiplicity of infection (MOI) = 100. Photopainting was performed *post facto* following fMCI and correlation analysis by bounding the identified cell(s) with a region of interest (ROI) and scanning the area with a λ = 405 nm diode laser (x20/0.8NA objective).

shRNA-silencing of connexin 36

For detailed information see Supplemental Experimental Procedures.

Immunohistochemistry

Islets were fixed at 4 °C overnight in paraformaldehyde (4%, wt/vol) before permeabilization (PBS + Triton 0.1%) and application of either guinea pig anti-insulin 1:200 (DAKO), mouse anti-glucagon 1:1000 (Sigma), rabbit anti-glucokinase 1:50 (Santa-Cruz), rabbit anti-Pdx1 1:50 (Rafiq, 2000), goat anti-Pdx1 1:2500 (Abcam), mouse anti-neurogenin-3 (Ngn3) 1:1000 (DSHB Hybridoma Product F25A1B3), rabbit anti-Tom20 1:250 (Santa Cruz Biotechnology), rabbit anti-Nkx6.1 1:250 (Sigma), rabbit anti-SERCA2 1:250 (Alomone Labs) or rabbit anti-PDI 1:200 (Cell Signaling Technology) antibodies for 24-48 h at 4°C. Staining was revealed following 2 h incubation at room temperature with secondary antibodies conjugated to Alexa Fluor-488, -568 and -633 (1:500) (Invitrogen). Connexin 36 (Cx36) staining was performed as above, but following 10 min fixation in ice-cold acetone and using rabbit anti-Cx36 1:50 (Zymed). To live image mitochondria, islets were incubated in 100 nM MitoTracker Red FM (Invitrogen) for 30 min.

Beta and alpha cell mass

For detailed information see Supplemental Experimental Procedures.

Necrosis and apoptosis assays

For detailed information see Supplemental Experimental Procedures.

Real-time PCR

Relative mRNA abundance was determined on an Applied Biosystems ABI 7500 Fast Real-Time PCR System using SYBR Green reagents and primers against connexin 36 (*Gjd2*) (GATTGGGAGGATCCTGTTGAC and AGGGCTAGGAAGACAGTAGAG). Gene expression was normalised to β-actin (CGAGTCGCGTCCACCC and CATCCATGGCGAACTGGTG) and fold-change in mRNA expression compared to control calculated using the $2^{-\Delta\Delta CT}$.

Correlation, similarity analyses and polar coordinates

Individual EYFP-expressing beta cells were identified using an ROI to produce a mask overlay of the imaged population. Correlation analyses were then performed in MATLAB on Hilbert-Huang transformed Ca^{2+} signals using binarization and matrix analyses, and statistical significance

assigned using non-deterministic (Monte-Carlo methods), as described (Hodson et al., 2010; Hodson et al., 2012). For detailed information see Supplemental Experimental Procedures.

Measurements of insulin secretion from isolated islets

Insulin secretion was measured using static incubation of islets (batches of 6-8) for 30 min in HEPES-bicarbonate buffer at 37°C containing the indicated glucose concentrations (da Silva Xavier et al., 2009). Insulin concentration in the supernatant was determined using a proprietary Homogeneous Time Resolved Fluorescence (HTRF)-based assay (Cisbio) according to the manufacturer's instructions.

Cytokines and glucolipotoxicity

Interleukin 1 beta (IL-1β), interleukin 6 (IL-6) and tumor necrosis factor alpha (TNF-α) (all from R&D Biosystems) were stored as stock solutions at -20 ^{0}C and used at 20 pg/ml, 40 pg/ml and 20 pg/ml, respectively (Maedler et al., 2004; O'Neill et al., 2013). For gluco(lipo)toxicity studies, cells were exposed to 33mM glucose and/or 0.5 mM BSA-conjugated palmitate for 48 h.

Statistical analyses

Data normality was assessed using the D'Agostino Pearson omnibus test. Pairwise comparisons were performed using paired or unpaired Student's t-test. Interactions between multiple treatments were determined using one-way or two-way ANOVA (adjusted for repeated measures as necessary), followed by pairwise comparisons with Bonferonni's or Tukey's posthoc tests. Analyses were conducted using R (R-project), Graphpad Prism 6.0 (Graphpad Software), IgorPro (Wavemetrics) and MATLAB (Mathworks), and results deemed significant at $P<0.05$. Unless otherwise stated, data are presented as the mean ± SEM.

REFERENCES

Ämmälä, C., Larsson, O., Berggren, P.-O., Bokvist, K., Juntti-Berggren, L., Kindmark, H., and Rorsman, P. (1991). Inositol trisphosphate-dependent periodic activation of a Ca2+-activated K+ conductance in glucose-stimulated pancreatic β-cells. Nature *353*, 849-852.

Andresen, V., Alexander, S., Heupel, W.M., Hirschberg, M., Hoffman, R.M., and Friedl, P. (2009). Infrared multiphoton microscopy: subcellular-resolved deep tissue imaging. Curr. Opin. Biotechnol. *20*, 54-62.

Benninger, R.K., Hutchens, T., Head, W.S., McCaughey, M.J., Zhang, M., Le Marchand, S.J., Satin, L.S., and Piston, D.W. (2014). Intrinsic islet heterogeneity and gap junction coupling determine spatiotemporal Ca(2)(+) wave dynamics. Biophys. J. *107*, 2723-2733.

Benninger, R.K., and Piston, D.W. (2014). Cellular communication and heterogeneity in pancreatic islet insulin secretion dynamics. Trends Endocrinol. Metab. *25*, 399-406.

Benninger, R.K., Zhang, M., Head, W.S., Satin, L.S., and Piston, D.W. (2008). Gap junction coupling and calcium waves in the pancreatic islet. Biophys. J. *95*, 5048-5061.

Bonifazi, P., Goldin, M., Picardo, M.A., Jorquera, I., Cattani, A., Bianconi, G., Represa, A., Ben-Ari, Y., and Cossart, R. (2009). GABAergic hub neurons orchestrate synchrony in developing hippocampal networks. Science *326*, 1419-1424.

Bosco, D., Armanet, M., Morel, P., Niclauss, N., Sgroi, A., Muller, Y.D., Giovannoni, L., Parnaud, G., and Berney, T. (2010). Unique arrangement of alpha- and beta-cells in human islets of Langerhans. Diabetes *59*, 1202-1210.

Broichhagen, J., Frank, J.A., and Trauner, D. (2015). A Roadmap to Success in Photopharmacology. Acc. Chem. Res. *51*, 6018-6021.

Broichhagen, J., Schönberger, M., Cork, S.C., Frank, J.A., Marchetti, P., Bugliani, M., Shapiro, A.M.J., Trapp, S., Rutter, G.A., Hodson, D.J., et al. (2014). Optical control of insulin release using a photoswitchable sulfonylurea. Nat. Commun. *5*, 5116.

Bullmore, E., and Sporns, O. (2009). Complex brain networks: graph theoretical analysis of structural and functional systems. Nat. Rev. Neurosci. *10*, 186-198.

da Silva Xavier, G., Loder, M.K., McDonald, A., Tarasov, A.I., Carzaniga, R., Kronenberger, K., Barg, S., and Rutter, G.A. (2009). TCF7L2 regulates late events in insulin secretion from pancreatic islet beta-cells. Diabetes *58*, 894-905.

Desarmenien, M.G., Jourdan, C., Toutain, B., Vessieres, E., Hormuzdi, S.G., and Guerineau, N.C. (2013). Gap junction signalling is a stress-regulated component of adrenal neuroendocrine stimulus-secretion coupling in vivo. Nat. Commun. *4*, 2938.

Farnsworth, N.L., and Benninger, R.K. (2014). New insights into the role of connexins in pancreatic islet function and diabetes. FEBS Lett. *588*, 1278-1287.

Farnsworth, N.L., Hemmati, A., Pozzoli, M., and Benninger, R.K. (2014). Fluorescence recovery after photobleaching reveals regulation and distribution of Cx36 gap junction coupling within mouse islets of langerhans. J. Physiol.

Farnsworth, N.L., Walter, R.L., Hemmati, A., Westacott, M.J., and Benninger, R.K. (2015). Low Level Pro-Inflammatory Cytokines Decrease Connexin36 Gap Junction Coupling in Mouse and Human Islets through Nitric Oxide Mediated Protein Kinase Cdelta. J. Biol. Chem.

Fonseca, S.G., Gromada, J., and Urano, F. (2011). Endoplasmic reticulum stress and pancreatic beta-cell death. Trends Endocrinol. Metab. *22*, 266-274.

Fujimoto, K., Hanson, P.T., Tran, H., Ford, E.L., Han, Z., Johnson, J.D., Schmidt, R.E., Green, K.G., Wice, B.M., and Polonsky, K.S. (2009). Autophagy regulates pancreatic beta cell death in response to Pdx1 deficiency and nutrient deprivation. J. Biol. Chem. *284*, 27664-27673.

Gerdes, J.M., Christou-Savina, S., Xiong, Y., Moede, T., Moruzzi, N., Karlsson-Edlund, P., Leibiger, B., Leibiger, I.B., Ostenson, C.G., Beales, P.L., et al. (2014). Ciliary dysfunction impairs beta-cell insulin secretion and promotes development of type 2 diabetes in rodents. Nat. Commun. *5*, 5308.

Head, W.S., Orseth, M.L., Nunemaker, C.S., Satin, L.S., Piston, D.W., and Benninger, R.K. (2012). Connexin-36 gap junctions regulate in vivo first- and second-phase insulin secretion dynamics and glucose tolerance in the conscious mouse. Diabetes *61*, 1700-1707.

Hodson, D.J., Mitchell, R.K., Bellomo, E.A., Sun, G., Vinet, L., Meda, P., Li, D., Li, W.H., Bugliani, M., Marchetti, P., et al. (2013). Lipotoxicity disrupts incretin-regulated human beta cell connectivity. J. Clin. Invest. *123*, 4182-4194.

Hodson, D.J., Molino, F., Fontanaud, P., Bonnefont, X., and Mollard, P. (2010). Investigating and Modelling Pituitary Endocrine Network Function. J. Neuroendocrinol., 1217-1225.

Hodson, D.J., Schaeffer, M., Romano, N., Fontanaud, P., Lafont, C., Birkenstock, J., Molino, F., Christian, H., Lockey, J., Carmignac, D., et al. (2012). Existence of long-lasting experience-dependent plasticity in endocrine cell networks. Nat. Commun. *3*, 605.

Hraha, T.H., Westacott, M.J., Pozzoli, M., Notary, A.M., McClatchey, P.M., and Benninger, R.K. (2014). Phase transitions in the multi-cellular regulatory behavior of pancreatic islet excitability. PLoS Comput. Biol. *10*, e1003819.

Katsuta, H., Aguayo-Mazzucato, C., Katsuta, R., Akashi, T., Hollister-Lock, J., Sharma, A.J., Bonner-Weir, S., and Weir, G.C. (2012). Subpopulations of GFP-marked mouse pancreatic beta-cells differ in size, granularity, and insulin secretion. Endocrinology *153*, 5180-5187.

Kiekens, R., In 't Veld, P., Mahler, T., Schuit, F., Van De Winkel, M., and Pipeleers, D. (1992). Differences in glucose recognition by individual rat pancreatic B cells are associated with intercellular differences in glucose-induced biosynthetic activity. J. Clin. Invest. *89*, 117-125.

Konstantinova, I., Nikolova, G., Ohara-Imaizumi, M., Meda, P., Kucera, T., Zarbalis, K., Wurst, W., Nagamatsu, S., and Lammert, E. (2007). EphA-Ephrin-A-mediated beta cell communication regulates insulin secretion from pancreatic islets. Cell *129*, 359-370.

Li, D., Chen, S., Bellomo, E.A., Tarasov, A.I., Kaut, C., Rutter, G.A., and Li, W.H. (2011). Imaging dynamic insulin release using a fluorescent zinc indicator for monitoring induced exocytotic release (ZIMIR). Proc. Natl. Acad. Sci. U. S. A. *108*, 21063-21068.

Luo, J., Deng, Z.-L., Luo, X., Tang, N., Song, W.-X., Chen, J., Sharff, K.A., Luu, H.H., Haydon, R.C., Kinzler, K.W., et al. (2007). A protocol for rapid generation of recombinant adenoviruses using the AdEasy system. Nat. Protoc. *2*, 1236-1247.

Maedler, K., Storling, J., Sturis, J., Zuellig, R.A., Spinas, G.A., Arkhammar, P.O., Mandrup-Poulsen, T., and Donath, M.Y. (2004). Glucose- and interleukin-1beta-induced beta-cell apoptosis requires Ca2+ influx and extracellular signal-regulated kinase (ERK) 1/2 activation and is prevented by a sulfonylurea receptor 1/inwardly rectifying K+ channel 6.2 (SUR/Kir6.2) selective potassium channel opener in human islets. Diabetes *53*, 1706-1713.

Mattis, J., Tye, K.M., Ferenczi, E.A., Ramakrishnan, C., O'Shea, D.J., Prakash, R., Gunaydin, L.A., Hyun, M., Fenno, L.E., Gradinaru, V., et al. (2012). Principles for applying optogenetic tools derived from direct comparative analysis of microbial opsins. Nat. Methods *9*, 159-172.

Meda, P., Atwater, I., Goncalves, A., Bangham, A., Orci, L., and Rojas, E. (1984). The topography of electrical synchrony among beta-cells in the mouse islet of Langerhans. Q. J. Exp. Physiol. *69*, 719-735.

Michau, A., Hodson, D.J., Fontanaud, P., Guillou, A., Espinosa-Carrasco, G., Molino, F., Peters, C.J., Robinson, I.C., Le Tissier, P., Mollard, P., et al. (2015). Metabolism regulates exposure of pancreatic islets to circulating molecules in vivo. Diabetes.

Nyman, L.R., Wells, K.S., Head, W.S., McCaughey, M., Ford, E., Brissova, M., Piston, D.W., and Powers, A.C. (2008). Real-time, multidimensional in vivo imaging used to investigate blood flow in mouse pancreatic islets. J. Clin. Invest. *118*, 3790-3797.

O'Neill, C.M., Lu, C., Corbin, K.L., Sharma, P.R., Dula, S.B., Carter, J.D., Ramadan, J.W., Xin, W., Lee, J.K., and Nunemaker, C.S. (2013). Circulating levels of IL-1B+IL-6 cause ER stress and dysfunction in islets from prediabetic male mice. Endocrinology *154*, 3077-3088.

Palti, Y., David, G.B., Lachov, E., Mida, Y.H., and Schatzberger, R. (1996). Islets of Langerhans generate wavelike electric activity modulated by glucose concentration. Diabetes *45*, 595-601.

Pancholi, J., Hodson, D.J., Jobe, K., Rutter, G.A., Goldup, S.M., and Watkinson, M. (2014). Biologically targeted probes for Zn2+: a diversity oriented modular “click-SNAr-click” approach. Chemical Science *5*, 3528-3535.

Pfisterer, C., Gruia, A., and Fischer, S. (2009). The mechanism of photo-energy storage in the Halorhodopsin chloride pump. J. Biol. Chem. *284*, 13562-13569.

Porat, S., Weinberg-Corem, N., Tornovsky-Babaey, S., Schyr-Ben-Haroush, R., Hija, A., Stolovich-Rain, M., Dadon, D., Granot, Z., Ben-Hur, V., White, P., et al. (2011). Control of Pancreatic β Cell Regeneration by Glucose Metabolism. Cell Metab. *13*, 440-449.
Pralong, W.F., Bartley, C., and Wollheim, C.B. (1990). Single islet beta-cell stimulation by nutrients: relationship between pyridine nucleotides, cytosolic Ca2+ and secretion. EMBO J. *9*, 53-60.
Proserpio, V., and Lonnberg, T. (2015). Single cell technologies are revolutionizing the approach to rare cells. Immunol. Cell Biol.
Rafiq, I. (2000). Glucose-stimulated Preproinsulin Gene Expression and Nuclear trans-Location of Pancreatic Duodenum Homeobox-1 Require Activation of Phosphatidylinositol 3-Kinase but Not p38 MAPK/SAPK2. J. Biol. Chem. *275*, 15977-15984.
Ravier, M.A., Guldenagel, M., Charollais, A., Gjinovci, A., Caille, D., Sohl, G., Wollheim, C.B., Willecke, K., Henquin, J.C., and Meda, P. (2005). Loss of connexin36 channels alters beta-cell coupling, islet synchronization of glucose-induced Ca2+ and insulin oscillations, and basal insulin release. Diabetes *54*, 1798-1807.
Reinbothe, T.M., Safi, F., Axelsson, A.S., Mollet, I.G., and Rosengren, A.H. (2014). Optogenetic control of insulin secretion in intact pancreatic islets with beta-cell-specific expression of Channelrhodopsin-2. Islets *6*.
Rickgauer, J.P., and Tank, D.W. (2009). Two-photon excitation of channelrhodopsin-2 at saturation. Proc. Natl. Acad. Sci. U. S. A. *106*, 15025-15030.
Rodriguez-Diaz, R., Speier, S., Molano, R.D., Formoso, A., Gans, I., Abdulreda, M.H., Cabrera, O., Molina, J., Fachado, A., Ricordi, C., et al. (2012). Noninvasive in vivo model demonstrating the effects of autonomic innervation on pancreatic islet function. Proc. Natl. Acad. Sci. U. S. A. *109*, 21456-21461.
Roma, L.P., Duprez, J., and Jonas, J.C. (2015). Glucokinase activation is beneficial or toxic to cultured rat pancreatic islets depending on the prevailing glucose concentration. Am. J. Physiol. Endocrinol. Metab. *309*, E632-E639.
Rutter, G.A., Pullen, T.J., Hodson, D.J., and Martinez-Sanchez, A. (2015). Pancreatic beta-cell identity, glucose sensing and the control of insulin secretion. Biochem. J. *466*, 203-218.
Salomon, D., and Meda, P. (1986). Heterogeneity and contact-dependent regulation of hormone secretion by individual B cells. Exp. Cell Res. *162*, 507-520.
Santos, R.M., Rosario, L.M., Nadal, A., Garcia-Sancho, J., Soria, B., and Valdeolmillos, M. (1991). Widespread synchronous [Ca2+]i oscillations due to bursting electrical activity in single pancreatic islets. Pflugers Arch. *418*, 417-422.
Speier, S., Nyqvist, D., Cabrera, O., Yu, J., Molano, R.D., Pileggi, A., Moede, T., Kohler, M., Wilbertz, J., Leibiger, B., et al. (2008). Noninvasive in vivo imaging of pancreatic islet cell biology. Nat. Med. *14*, 574-578.
Squires, P.E., Persaud, S.J., Hauge-Evans, A.C., Gray, E., Ratcliff, H., and Jones, P.M. (2002). Co-ordinated Ca(2+)-signalling within pancreatic islets: does beta-cell entrainment require a secreted messenger. Cell Calcium *31*, 209-219.
Stolovich-Rain, M., Enk, J., Vikesa, J., Nielsen, Finn C., Saada, A., Glaser, B., and Dor, Y. (2015). Weaning Triggers a Maturation Step of Pancreatic β Cells. Dev. Cell *32*, 535-545.
Stozer, A., Gosak, M., Dolensek, J., Perc, M., Marhl, M., Rupnik, M.S., and Korosak, D. (2013). Functional connectivity in islets of Langerhans from mouse pancreas tissue slices. PLoS Comput. Biol. *9*, e1002923.
Subach, F.V., Patterson, G.H., Renz, M., Lippincott-Schwartz, J., and Verkhusha, V.V. (2010). Bright monomeric photoactivatable red fluorescent protein for two-color super-resolution sptPALM of live cells. J. Am. Chem. Soc. *132*, 6481-6491.
Szabat, M., Luciani, D.S., Piret, J.M., and Johnson, J.D. (2009). Maturation of adult beta-cells revealed using a Pdx1/insulin dual-reporter lentivirus. Endocrinology *150*, 1627-1635.
Tarasov, A.I., Semplici, F., Ravier, M.A., Bellomo, E.A., Pullen, T.J., Gilon, P., Sekler, I., Rizzuto, R., and Rutter, G.A. (2012). The mitochondrial Ca2+ uniporter MCU is essential for glucose-induced ATP increases in pancreatic beta-cells. PLoS ONE *7*, e39722.
Taylor, Brandon L., Liu, F.-F., and Sander, M. (2013). Nkx6.1 Is Essential for Maintaining the Functional State of Pancreatic Beta Cells. Cell Reports *4*, 1262-1275.

Thorens, B., Tarussio, D., Maestro, M.A., Rovira, M., Heikkila, E., and Ferrer, J. (2014). Ins1 knock-in mice for beta cell-specific gene recombination. Diabetologia.

Varadi, A., Grant, A., McCormack, M., Nicolson, T., Magistri, M., Mitchell, K.J., Halestrap, A.P., Yuan, H., Schwappach, B., and Rutter, G.A. (2006). Intracellular ATP-sensitive K+ channels in mouse pancreatic beta cells: against a role in organelle cation homeostasis. Diabetologia *49*, 1567-1577.

Varo, G., Zimanyi, L., Fan, X., Sun, L., Needleman, R., and Lanyi, J.K. (1995). Photocycle of halorhodopsin from Halobacterium salinarium. Biophys. J. *68*, 2062-2072.

Zhang, F., Wang, L.P., Brauner, M., Liewald, J.F., Kay, K., Watzke, N., Wood, P.G., Bamberg, E., Nagel, G., Gottschalk, A., et al. (2007). Multimodal fast optical interrogation of neural circuitry. Nature *446*, 633-639.

Zhang, M., Fendler, B., Peercy, B., Goel, P., Bertram, R., Sherman, A., and Satin, L. (2008a). Long lasting synchronization of calcium oscillations by cholinergic stimulation in isolated pancreatic islets. Biophys. J. *95*, 4676-4688.

Zhang, Q., Galvanovskis, J., Abdulkader, F., Partridge, C.J., Gopel, S.O., Eliasson, L., and Rorsman, P. (2008b). Cell coupling in mouse pancreatic beta-cells measured in intact islets of Langerhans. Philos. Transact. A Math. Phys. Eng. Sci. *366*, 3503-3523.

ACKNOWLEDGEMENTS

N.R.J. was supported by a Diabetes UK RW and JM Collins Studentship (12/0004601). J.B. was supported by a European Foundation for the Study of Diabetes (EFSD) Albert Renold Young Scientist Fellowship and a Studienstiftung des deutschen Volkes PhD Studentship. D.T. was supported by an Advanced Grant from the European Research Commission (268795). G.A.R. was supported by Wellcome Trust Senior Investigator (WT098424AIA) and Royal Society Wolfson Research Merit Awards, and by MRC Programme (MR/J0003042/1), Biological and Biotechnology Research Council (BB/J015873/1) and Diabetes UK Project (11/0004210) grants. G.A.R. and M.W. acknowledge COST Action TD1304 Zinc-Net. D.J.H. was supported by Diabetes UK R.D. Lawrence (12/0004431) and EFSD/Novo Nordisk Rising Star Fellowships, and an MRC Project Grant (MR/N00275X/1) with G.A.R. D.J.H and G.A.R. were supported by Imperial Confidence in Concept (ICiC) Grants. JF was supported by an MRC Programme grant (MR/L02036X/1). LP provided human islets through collaboration with the Diabetes Research Institute, IRCCS San Raffaele Scientific Institute (Milan), within the European islet distribution program for basic research supported by JDRF (1-RSC-2014-90-I-X). PM and MB were supported by the Innovative Medicine Initiative Joint Undertaking under grant agreement no. 155005 (IMIDIA), resources of which are composed of financial contribution from the European Union's Seventh Framework Programme (FP7/2007-2013) and EFPIA companies in kind contribution, and by the Italian Ministry of University and Research (PRIN 2010-2012). DB and EB provided human islets through the European Consortium for Islet Transplantation sponsored by JDRF (1-RSC-2014-100-I-X). We are grateful to Drs Richard K.P. Benninger (University of Colorado Denver), Francois Molino (Université Montpellier II) and Stephen Rothery (FILM Facility, Imperial College London) for useful discussion. The authors have no conflicts of interest to disclose.

AUTHOR CONTRIBUTIONS

N.R.J., G.A.R. and D.J.H. conceived and designed the experiments. N.R.J, R.K.M, E.H., M.P.P., F.S. and D.J.H. conducted the experiments. J.F. provided reagents and intellectual input. L.P., P.M., M.B., D.B., E.B. isolated and provided human islet of Langerhans. P.D., M.W., J.B. and D.T. designed, synthesized and provided chemical reagents. N.R.J., G.A.R. and D.J.H. wrote the paper with input from all the authors.

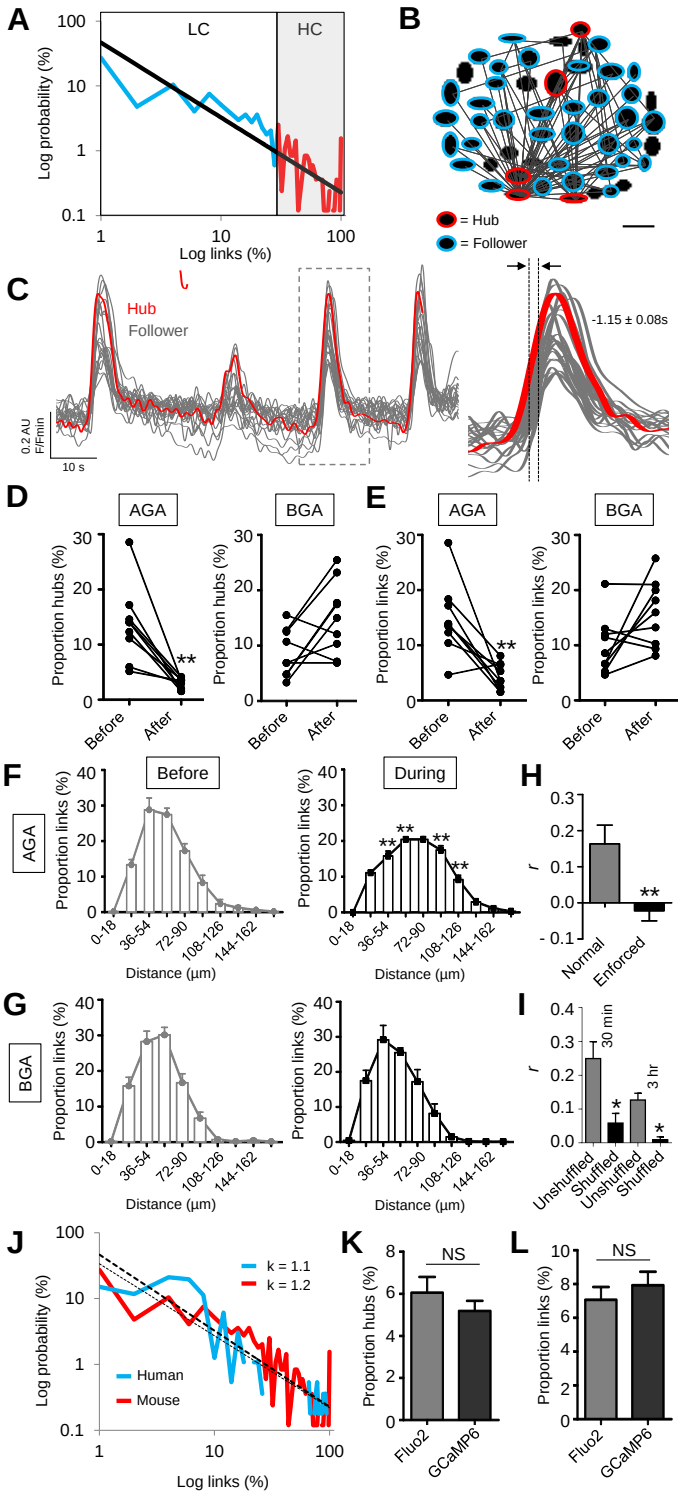

Fig. 1. Functional mapping of beta cell population dynamics (A) At elevated glucose (11 mM), islets house a scale-free network where a few (< 10 %) beta cells host the majority of correlated links (P<0.01), as shown by the power law-fitted probability distribution (LC, low connectivity range; HC, high connectivity range) (R^2 = 0.72) (*n* = 12 recordings from 5 animals). To better demonstrate the distribution, a log-log scale is used to convert the power-law into a linear relationship. (B) Representative functional connectivity map displaying the x-y position of analyzed cells and their links (followers, blue; hubs, red) (scale bar = 20 μm). (C) Representative trace showing that hub (red) activity tends to precede and outlast that of follower cells (mean lag value calculated from *n* = 5 recordings from 3 animals). (D) Treatment of islets with the gap junction blocker 18α-glycyrrhetinic acid (AGA; 20 μM) (left), but not its inactive analog glycyrrhizic acid (BGA; 20 μM) (right) reduces the proportion of hubs (*n* = 9 recordings from 5

animals) (before, islet in control buffer; after, same islet in the presence of either AGA or BGA). (E) As for (D) but the percentage (%) of correlated links. (F and G) Gap junction blockade increases the length between correlated links (n = 9 recordings from 5 animals). (H) Wiring patterns are statistically stable upon re-recording after 30 min, as determined against the same islet but with enforced dissimilarity (n = 8 recordings from 5 animals). (I) Wiring patterns are statistically stable upon re-recording after 30 min (Fluo2) and 3 hrs (GCaMP6), as compared to the randomly-shuffled matrix for each islet (n = 4-6 recordings from 2-3 animals). (J) As for (A) but showing almost identical link-probability distributions in mouse and human islets, as shown by the exponent values (κ) for the fitted power laws (n = 8 recordings from 3 donors). (K-L) Imaging using GCaMP6 and Fluo2 return similar hub and link proportions (n = 12 recordings from 4-6 animals). Data are means ± SEM.*P<0.05 and **P<0.01 and NS, non-significant.

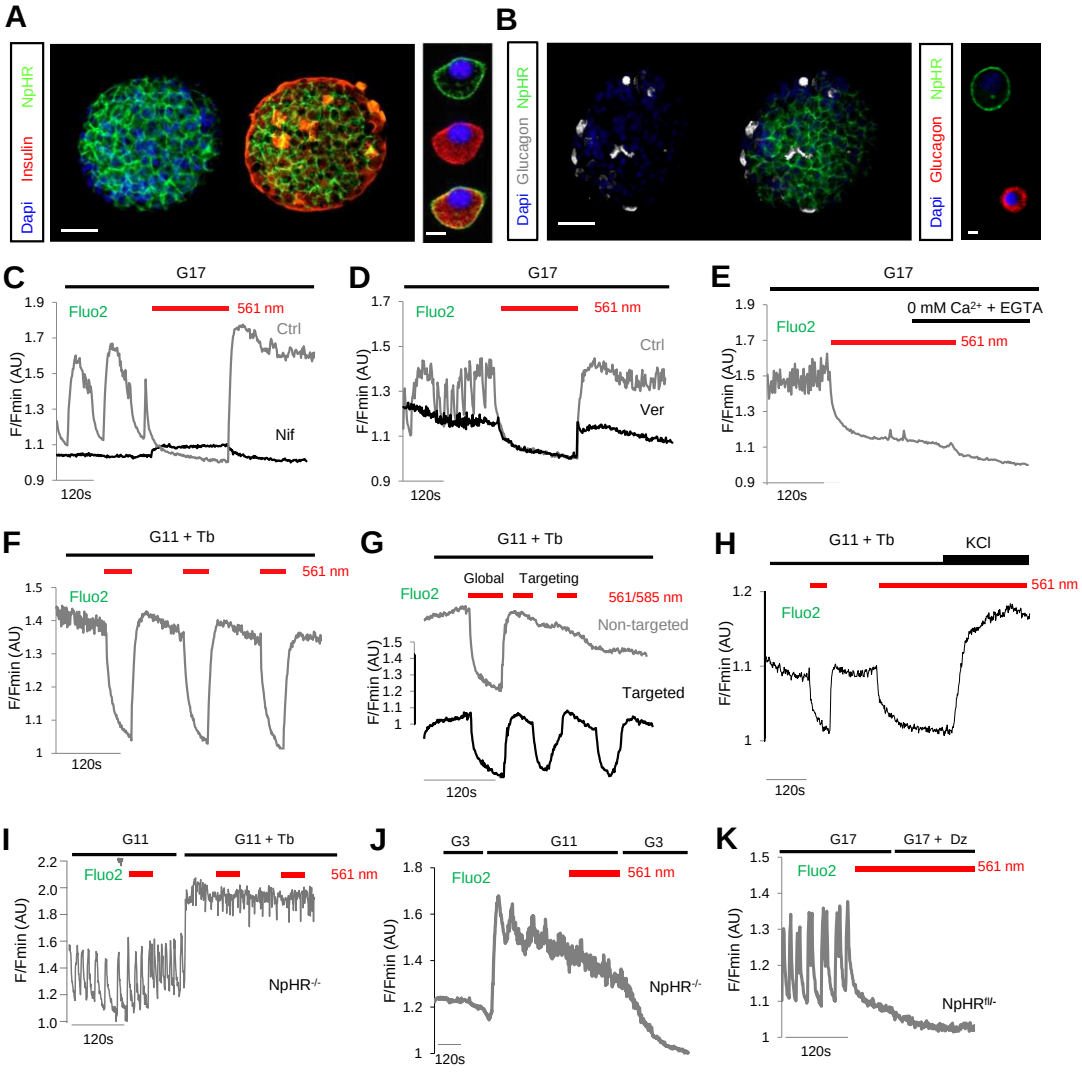

Fig. 2. Reversible and repeated silencing of beta cell Ca^{2+}-spiking activity. (A) Immunostaining for insulin showing membrane-localized expression of eNpHR3.0-EYFP in beta cells (Dapi, nuclei) (*n* = 3 preparations). (B) As for (A), but immunostaining for glucagon showing absence of eNpHR3.0-EYFP in alpha cells (*n* = 3 preparations). Scale bar = 50 µm (or 10 µm for dissociated cells). (C) Reversible silencing of beta cell Ca^{2+} oscillations in eNpHR3.0-expressing islets in response to illumination with λ = 561 nm (*n* = 5 recordings). Treatment of islets with nifedipine 50 µM (Nif; black trace) abolishes the rebound in Ca^{2+} upon inactivation of eNpHR3.0 (*n* = 5 recordings) (traces are from different islets). (D) As for (C) but in the presence of verapamil 10 µM (Ver; black trace) (*n* = 5 recordings) (traces are from different islets). (E) Perifusion of islets with zero Ca^{2+} supplemented with EGTA was able to prevent recovery of $[Ca^{2+}]_i$ in islets following silencing (*n* = 5 recordings). (F) Beta cell population Ca^{2+}-spiking activity can be repeatedly silenced following exposure to λ = 561 nm (*n* = 3 recordings). (G) Global silencing (λ = 561 nm) induced a decrease in intracellular Ca^{2+} concentrations ($[Ca^{2+}]_i$) throughout the islet, whereas a diffraction-limited laser (λ = 585 nm) only silenced $[Ca^{2+}]_i$ in the targeted area (*n* = 3 recordings). (H) Silencing can be overcome using the depolarizing agent KCl 30 mM to re-activate VDCC (*n* = 6 recordings). (I-J) Wild-type islets ($NpHR^{-/-}$) do not respond to illumination with decreases in $[Ca^{2+}]_i$ (*n* = 5 recordings). (K) Diazoxide (Dz) 100 µM is unable to further suppress $[Ca^{2+}]_i$ in eNpHR3.0-silenced islets (*n* = 5 recordings). Where indicated, tolbutamide (Tb) 100 µM was added to maintain a stable plateau from which to better detect silencing. G17, glucose 17 mM; G11, glucose 11 mM.; G3, glucose 3 mM.

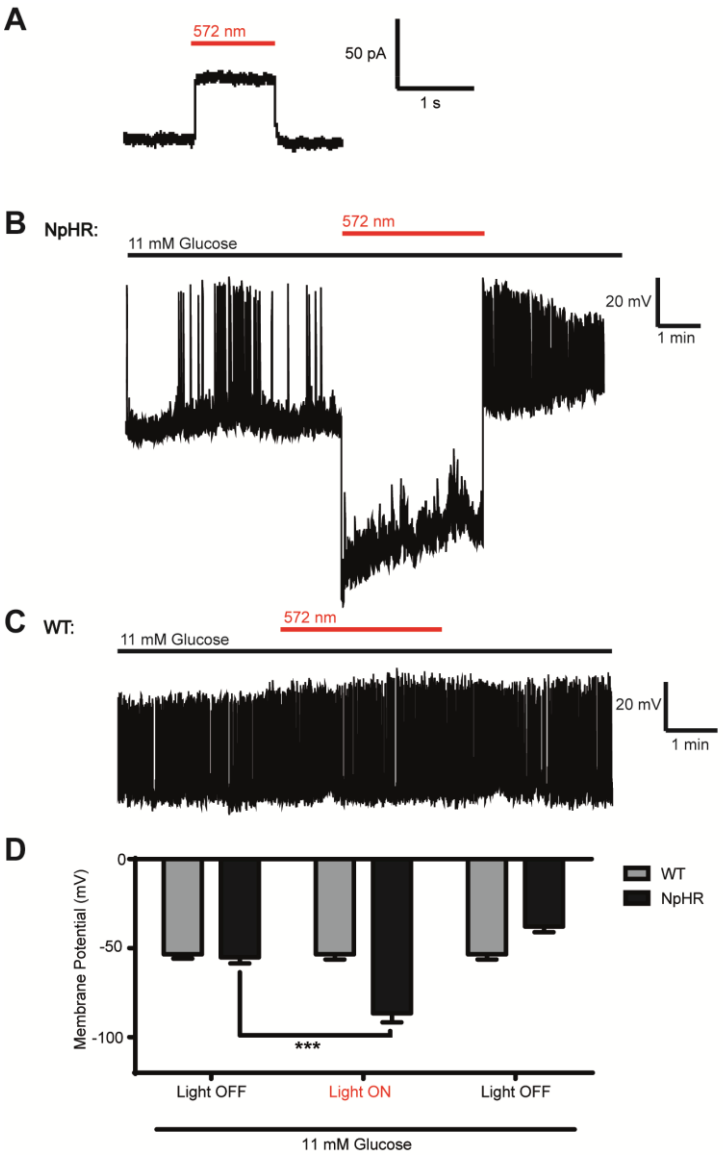

Fig. 3. Yellow light hyperpolarizes eNpHR3.0-expressing pancreatic beta-cells. (A) Voltage clamp (whole cell) recording of an eNpHR3.0-expressing beta cell showing induction of photocurrents with yellow light (λ = 572 nm). (B-D) Representative current clamp (perforated patch) recordings showing reversible membrane hyperpolarization with yellow light (λ = 572 nm) in an eNpHR3.0-expressing, but not wild-type (WT) beta cell. In all cases, *n* = 6-11 cells. Data are means ± SEM. ***P<0.001.

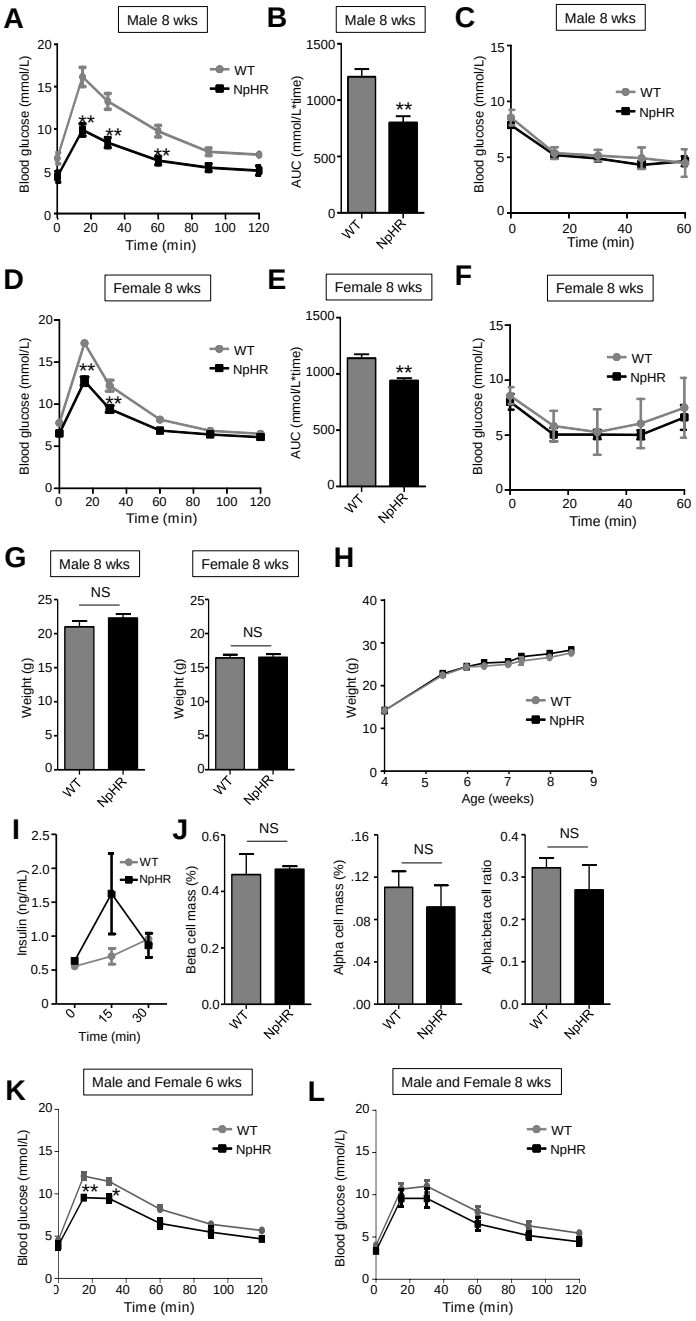

Fig. 4. Glucose homeostasis in eNpHR3.0 mice. (A-B) Glucose tolerance is improved in male 8 wk Ins1Cre$^{+/-}$;eNpHR3.0-EYFP$^{fl/-}$(NpHR) animals (n = 7) compared to Ins1Cre$^{-/-}$;eNpHR3.0-EYFP$^{fl/-}$ (wild type, WT) littermates (n = 7) (*i.e.* activation of Ins1Cre on an eNpHR3.0-EYFP background), as assessed using IPGTT. (C) Insulin sensitivity is similar in male NpHR mice animals and WT littermates (n = 6-11), as determined using ITT. (D-E) As for (A-B) but female 8 wk mice (n = 7-9). (F) As for (C) but female 8 wk (n = 4). (G-H) Fasting body weight and growth curves (non-fasted) are similar in WT and NpHR animals (n = 9-13). (I) *In vivo* insulin release tended to be increased in NpHR compared to WT animals at 15 min post-IP glucose injection (n = 4). (J) Beta cell mass, alpha cell mass and alpha:beta cell ratio are similar in WT and NpHR animals (n = 3). (K-L) As for (A-B) but glucose tolerance in 6 and 8 wk Ins1Cre$^{+/-}$;eNpHR3.0-EYFP$^{fl/-}$(NpHR) (n = 3-4) compared to Ins1Cre$^{+/-}$;eNpHR3.0-EYFP$^{-/-}$ (wild type, WT) animals (n = 8) (*i.e.* activation of eNpHR3.0-EYFP on an Ins1Cre-background). Data are means ± SEM. **P<0.01 and NS, non-significant.

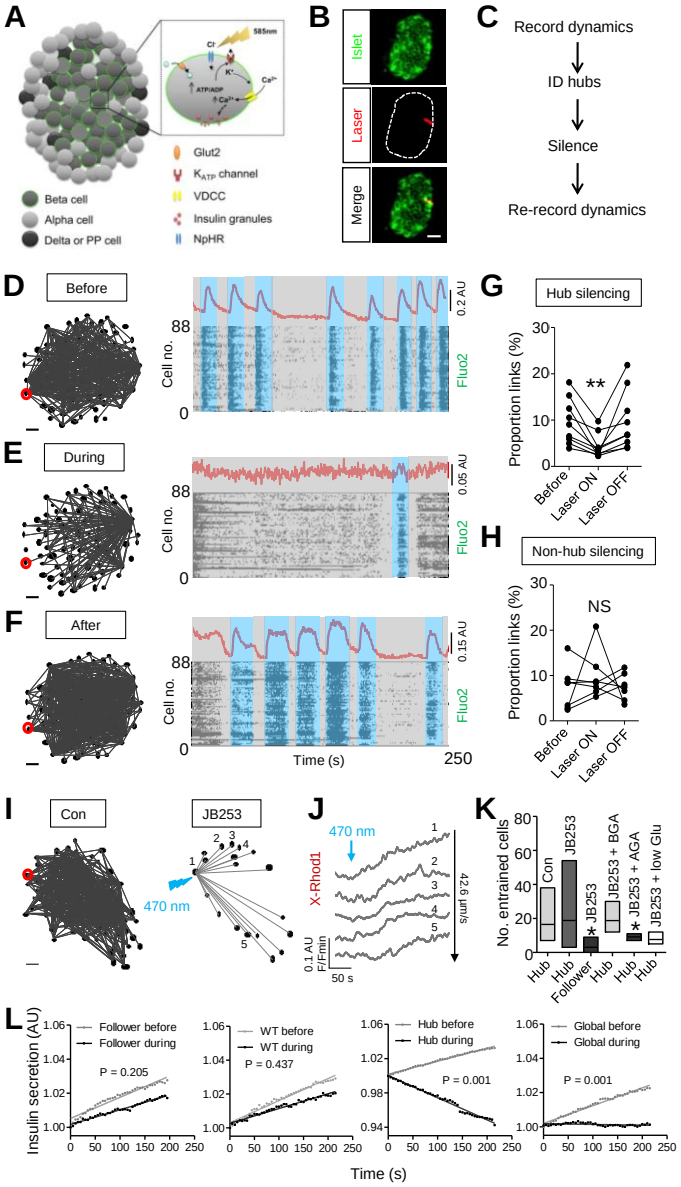

Fig. 5. Real-time analysis and targeting of beta cell hubs. (A-B) Schematic showing the effects of eNpHR3.0 activation upon beta cell Ca^{2+} signaling (A), and snapshot showing placement of a diffraction-limited laser spot over a discrete islet region (B) (scale bar, 25 µm; image cropped to display a single islet). (C) Experimental flowchart for real-time manipulation of hub function. (D to F) Representative functional connectivity map and activity plots at high glucose (11 mM), before (D), during (E) and after (F) optogenetic silencing (identified hub cell; red). A representative Ca^{2+} trace is displayed above. (G-H) Summary data showing a reversible collapse in the proportion of correlated cell links following hub (G), but not follower (H) silencing (n = 7-9 recordings from 4 animals). (I-K) Representative experiment showing cell-cell entrainment patterns (I) and representative Ca^{2+} rises in linked cells (J) following photopharmacological stimulation of an identified hub (red) at 3 mM glucose using JB253 (50 µM) (low Glu = 1 mM glucose). Box and whiskers plot shows the range and mean number of hub- or follower-entrained cells under normal (high glucose) conditions, and following targeted stimulation using JB253 in the presence of control (Con; 3 mM glucose), BGA, AGA and low glucose (1 mM) (K) (n = 4-7 recordings from 3-4 animals). (L) Insulin secretion measured using JP-107 is unaffected following illumination of follower cells or wild-type (WT) islets, but suppressed in response to hub or islet (global) shutdown (mean traces shown) (n = 8 islets from 4 animals). Scale bars = 20 µm. Data are means ± SEM. *P<0.05 and NS, non-significant.

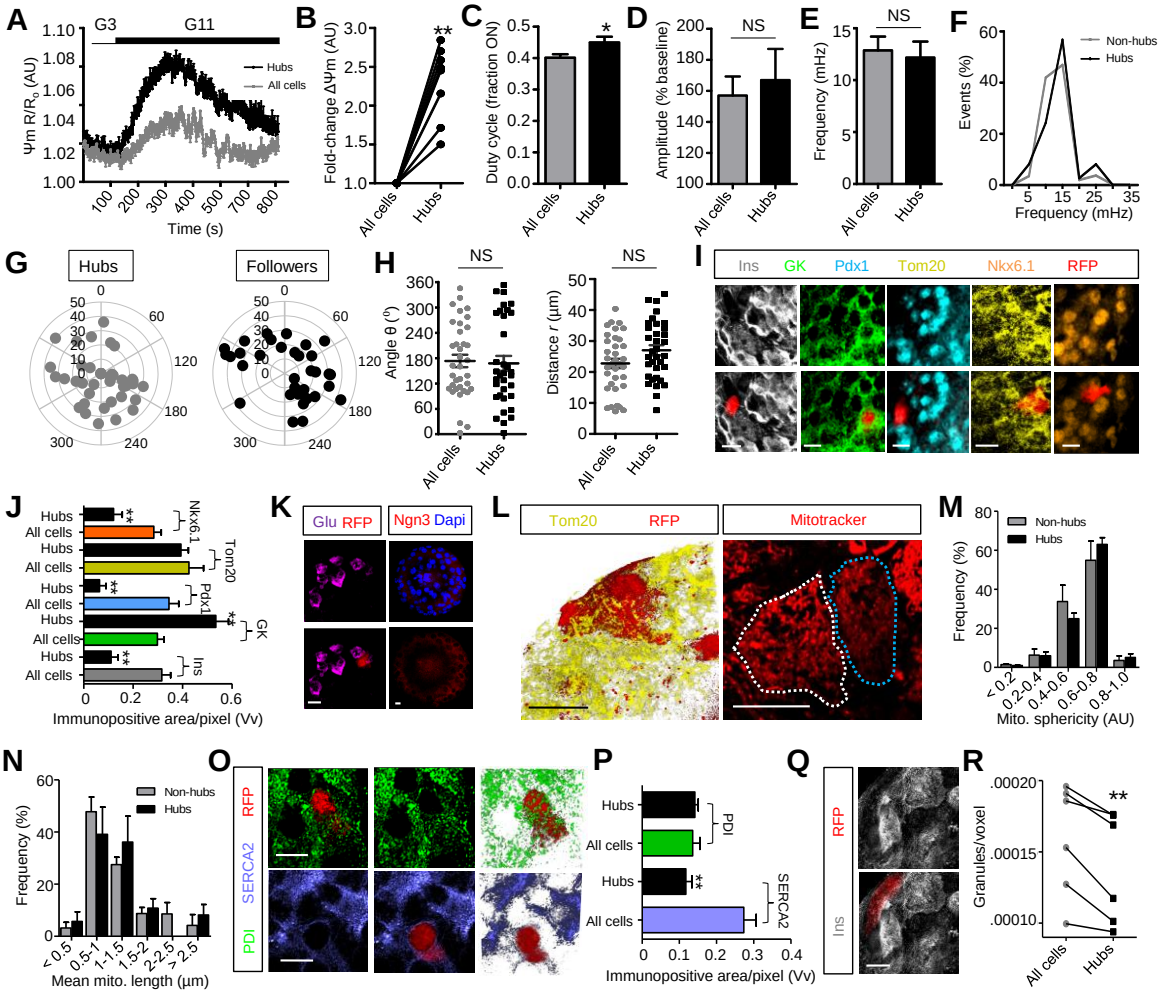

Fig. 6. Phenotypic profiling of hub cell function. (A-B) Hubs display elevated mitochondrial potential (Ψm) compared to the rest of the population, as measured using TMRE to label active mitochondria (n = 9 recordings from 3 animals) (G3, glucose 3 mM; G11, glucose 11 mM). (C-F) Duty cycle (*i.e.* fraction spent 'ON') (C), and Ca^{2+} oscillation amplitude (D) and frequency (E-F) are similar in hubs and followers (n = 8 recordings from 4 animals). (G-H) Polar coordinates showing that hub distribution is not spatially-biased *versus* followers (angle θ and distance r from the islet center 0,0 are shown in the bar graphs). (I-J) PA-TagRFP-identified hubs (red; RFP) express less insulin (Ins), less Pdx1, less Nkx6.1, more glucokinase (GK), and normal Tom20 compared to the rest of the population (n = 5-9 hubs from 3-4 animals). (K) Hubs were not immunopositive for glucagon (Glu), and Neurogenin 3 (Ngn3) expression was largely undetectable in the adult islet. (L-N) High resolution Z-projections of Tom20- and MitoTracker-stained islets (L) reveal normal mitochondrial sphericity (M) and length (N) (white-dashed line, hub; blue-dashed line, non-hub) (3D render shown for TOM20 and Z-projection for MitoTracker) (n = 6 hubs from 3 animals). (O-P) As for (L-N), but staining for PDI and SERCA2 showing normal ER abundance and lowered Ca^{2+}-ATPase content in hubs (Z-projection, left; 3D render, right) (n = 4-5 hubs from 3 animals). (Q-R) High-resolution snapshot of insulin staining (Q) showing a reduction in granule content in hubs (red) (R) (n = 6 hubs from 3 animals). Scale bars = 12.5 μm. Data are means ± SEM. *P<0.05, **P<0.01 and NS, non-significant.

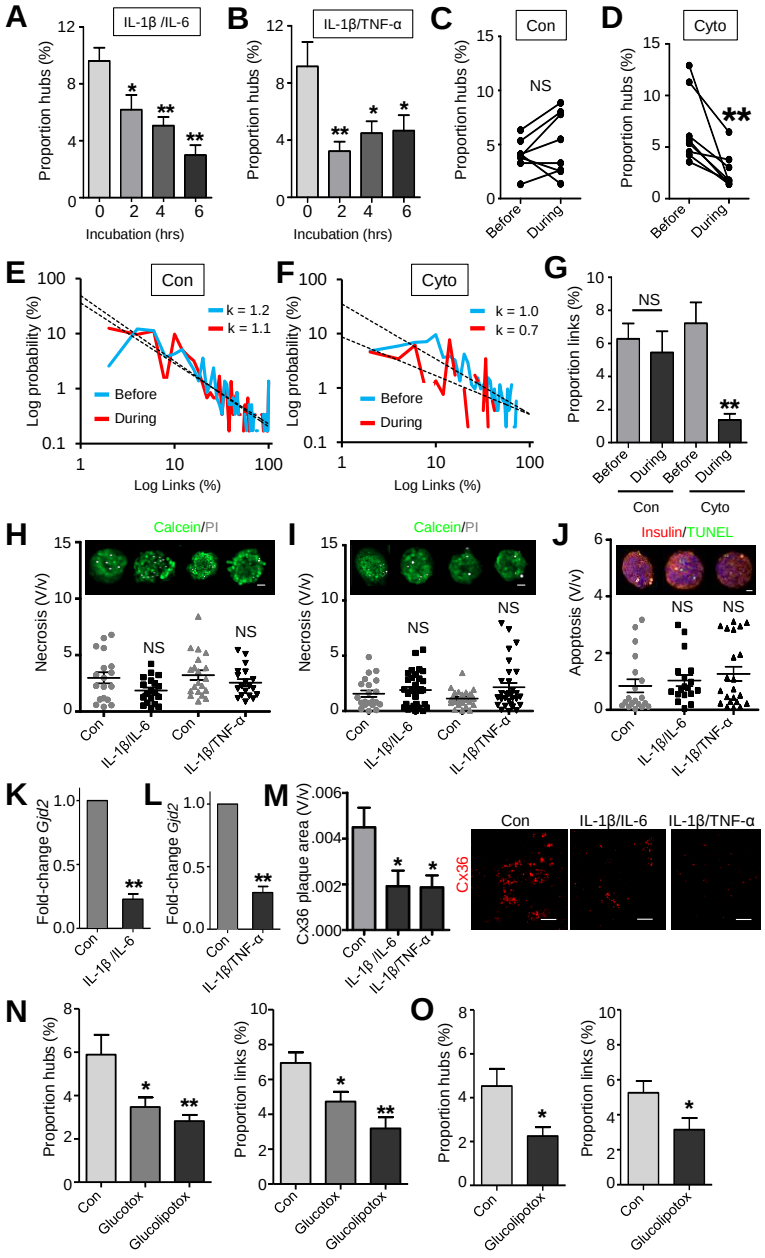

Fig. 7. Disruption of hubs by pro-inflammatory and glucolipotoxic insults. (A-B) IL-1β/IL-6 and IL-1β/TNF-α reduce hub number after 2 h (*n* = 6 islets from 3 animals). (C-D) Cytokine (Cyto; IL-1β/IL-6) decreases hub number in real-time (*n* = 8 from 4 animals). (E-F) Cytokine alters the distribution of correlated links and power-law scaling exponent (*k*) value, indicating a decreased number of cells in the high connectivity (*i.e.* hub) range (*n* = 8 from 4 animals) (R^2 = 0.38–0.74). The power-law was log-log transformed to a linear relationship to better demonstrate the distribution. (G) Cytokine (IL-1β/IL-6**)** exposure dramatically reduces the proportion of correlated links. (H to I) Application of IL-1β/IL-6 or IL-1β/TNF-α for 2 h (H) or 4 h (I) is not cytotoxic (*n* = 21 islets per condition from 6 animals) (scale bar, 25 µm). (J) 2 h application of IL-1β/IL-6 or IL-1β/TNF-α does not induce apoptosis (*n* = 18-20 islets from 5 animals). (K-L) IL-1β/IL-6 and IL-1β/TNF-α decrease connexin 36 (*GJD2)* mRNA levels (*n* = 10 animals). (M) IL-1β/IL-6 and IL-1β/TNF-α reduce the number of immunostained gap junction (Cx36) plaques (*n* = 9-12 islets from 6 animals) (scale bar, 12.5 µm). (N) Glucotoxicity (Glucotox) and glucolipotoxicity (Glucolipotox) reduce the proportion of hubs and correlated links in mouse islets (*n* = 6 animals). (O) As for (N) but showing effects of glucolipotoxicity-alone on human islets (*n* = 5 donors). Data are means ± SEM. *P<0.05, **P<0.01 and NS, non-significant.